Published in final edited form as:
Mol Cell Neurosci. 2014 January ; 58: 76–84. doi:10.1016/j.mcn.2013.12.003.

The schizophrenia susceptibility gene DTNBP1 modulates AMPAR synaptic transmission and plasticity in the hippocampus of juvenile DBA/2J mice

Ian J Orozco[1,4], **Peter Koppensteiner**[1], **Ipe Ninan**[2], and **Ottavio Arancio**[1,3]

[1]Department of Pathology and Cell Biology and Taub Institute for Research on Alzheimer's Disease and the Aging Brain, Columbia University, 630 W 168th St., New York, NY 10032, USA

[2]Department of Psychiatry, New York University Langone Medical Center, New York, NY 10016, USA

Abstract

The dystrobrevin binding protein (DTNBP) 1 gene has emerged over the last decade as a potential susceptibility locus for schizophrenia. While no causative mutations have been found, reduced expression of the encoded protein, dysbindin, was reported in patients. Dysbindin likely plays a role in the neuronal trafficking of proteins including receptors. One important pathway suspected to be affected in schizophrenia is the fast excitatory glutamatergic transmission mediated by AMPA receptors. Here, we investigated excitatory synaptic transmission and plasticity in hippocampal neurons from dysbindin-deficient sandy mice bred on the DBA/2J strain. In cultured neurons an enhancement of AMPAR responses was observed. The enhancement of AMPAR-mediated transmission was confirmed in hippocampal CA3-CA1 synapses, and was not associated with changes in the expression of GluA1–4 subunits nor an increase in GluR2-lacking receptor complexes. Lastly, an enhancement in LTP was also found in these mice. These data provide compelling evidence that dysbindin, a widely suspected susceptibility protein in schizophrenia, is important for AMPAR-mediated synaptic transmission and plasticity in the developing hippocampus.

Keywords

DTNBP1; dysbindin; schizophrenia; AMPAR; LTP

Introduction

The DTNBP1 gene has generated much interest due to its link to schizophrenia following a seminal Irish family-based association analysis (Straub et al., 2002). While dysbindin expression was found to be reduced in the hippocampus and cortex of schizophrenia patients

[3]Corresponding author: Current address: 630 West 168th Street, P&S 12-420D, New York, NY 10032, USA Telephone: +001 212-342-0533, oa1@columbia.edu.
[4]Present address: Max Delbrück Center (MDC) & Leibniz-Institut für Molekulare Pharmakologie (FMP), Berlin, Germany. ian.orozco@mdc-berlin.de

Financial Disclosures. The authors have no financial disclosures.

(Talbot et al., 2004; Tang et al., 2009a; Weickert et al., 2008), how dysbindin modulates the pathogenesis of the disease remains unclear. While schizophrenia has often been modeled as a neurodevelopmental disorder (Rapoport et al., 2005), several lines of evidence suggest that dysbindin may have a role in brain development. Imaging studies in children found that genetic variation in DTNBP1 was associated with changes in grey and white brain matter volume (Tognin et al., 2011) and hyper-activation of particular regions during visual processing (Mechelli et al., 2010). In rodents, dysbindin expression is highest during embryonic stages (Ghiani et al., 2010; Ito et al., 2010) while reduction of dysbindin in cultured neurons led to abnormalities in neurite growth and dendritic morphology (Ghiani et al., 2010; Ito et al., 2010; Kubota et al., 2009; Ma et al., 2011). Dysbindin is likely involved in protein trafficking along the endosomal-lysosomal pathway (Di Pietro et al., 2006; Gokhale et al., 2012; Larimore et al., 2011) as it was shown to be a component of the biogenesis of lysosome-related organelles (BLOC)-1 complex (Li et al., 2003; Starcevic and Dell'Angelica, 2004) and to interact with the adaptor-protein 3 (AP-3) complex (Hikita et al., 2009; Taneichi-Kuroda et al., 2009). Dysbindin has been shown to modulate the membrane surface expression of at least two receptor classes, NMDAR (Tang et al., 2009b) and D2R (Iizuka et al., 2007; Ji et al., 2009; Marley and von Zastrow, 2010).

Besides a potential role in development and receptor trafficking, fractionation studies with human tissue revealed that dysbindin was present in hippocampal synapses suggesting a role in neurotransmission (Talbot et al., 2004; Talbot et al., 2011). Magnetic resonance imaging revealed that a mouse model lacking dysbindin due to a spontaneous deletion in the DTNBP 1 gene (Li et al., 2003), named sandy, displayed alterations in hippocampal activity (Lutkenhoff et al., 2012). This is consistent with studies reporting altered glutamatergic transmission in acute brain slices from the sandy mice (Chen et al., 2008; Tang et al., 2009b). Whether these defects represent primary or secondary consequences, due to compensatory mechanisms expression, remains unclear. No electrophysiology studies have been performed in primary neurons from sandy mice where cell autonomous phenotypes can be identified. To explore whether dysbindin affects fast glutamatergic synaptic transmission mediated by the AMPAR classes of receptors, we first analyzed hippocampal cultures prepared from sandy animals lacking dysbindin expression and uncovered a previously unidentified defect in AMPAR function. We also found that loss of dysbindin led to enhanced CA3-CA1 AMPAR-mediated synaptic transmission and long term plasticity in acute hippocampal slices from juvenile animals. Altogether, these findings suggest that dysbindin expression may affect hippocampal based cognitive processes by influencing AMPAR function during juvenile brain development.

Material and methods

Sandy mice breeding

The sandy mice were acquired from Dr. Richard Swank (Buffalo, New York) and maintained on the original DBA/2J background strain. The animals were housed in a facility on the Columbia University Medical Center campus under approved IACUC protocol. Control (+/+) and sandy (−/−) animals littermates were used for analysis and obtained from breedings between heterozygote animals for the sandy allele. Genotypes were determined by PCR analysis of genomic DNA purified from tail biopsies (Li et al., 2003).

Chemicals and antibodies

Reagents were purchased from the following commercial vendors. Tocris Bioscience: tetrodotoxin. Sigma-Aldrich: CNQX, D-APV, bicuculline, spermine, picrotoxin, poly-D-lysine, AMPA, 5-fluoro-2′-deoxyuridine, kynuerenic acid. Life Technologies: FM 4–64,

mouse laminin, Neurobasal A media, B27 supplement. Millipore: GluA1–4 and GluA1P antibodies.

Preparation of primary hippocampal cultures

Hippocampi removed from +/+ and sdy/sdy pups (P1–2) were trypsin-treated (0.25%) and triturated before plating in high glucose DMEM with 10% fetal calf serum onto glass cover slips coated with poly D-lysine (20 μg/mL) and mouse laminin (10 μg/mL). The cells were maintained in an incubator at 37°C with 5% CO_2. The next day, the medium was replaced with Neurobasal A containing 2% B27 supplement, 1% FCS, 0.4 mM glutamine, 24 μM β-mercaptoethanol, 70 μM uridine, 30 μM 5-fluoro-2′-deoxyuridine, and 0.5 mM kynuerenic acid. Until analysis, the cells were maintained in the incubator without further media changes.

FM dye assay

Hippocampal cells (DIV 17–21) were used. Cover slips were assembled into a Chamlide recording chamber (Life Cell Instruments, South Korea) containing two platinum electrodes. The cells were exposed to 15 μM FM4–64 in HEPES-buffered NaCl solution (pH 7.4) containing (in mM): 119 NaCl, 2.5 KCl, 2 $CaCl_2$, 2 $MgCl_2$, 25 HEPES, 30 glucose, 10 μM CNQX and 40 μM D-APV for 1 minute. The cells were stimulated with 600 1ms pulses at a frequency of 10Hz. After stimulation, cells were given 2 minutes to allow for endocytosis. The cells were then washed for 10 minutes with HEPES-buffered NaCl solution. After washing, a region with individually identifiable fluorescent puncta was selected (Olympus IX81). For time-lapse imaging, pictures (200ms exposure, 4×4 binning) were acquired every 10s. Under constant perfusion (2 mL/min), several images were first acquired to evaluate photobleaching and then the cells were stimulated with 1200 pulses (10Hz, 60s). Following a brief rest period, the cells were stimulated with another 1200 pulses (10Hz, 60s) to ensure complete dye de-staining. For offline analysis, labeled boutons were hand selected by size (1.5 μm × 1.5 μm) (Ryan and Smith, 1995). Experiments where the cover slip had moved during imaging were discarded from analysis. Using ImageJ software, regions of interest (ROIs) were made for each bouton. ROIs were also selected nearby labeled boutons to measure non-synaptic fluorescence, which was then subtracted from all bouton fluorescence values. The background fluorescence of each bouton acquired at the end of the stimulation was subtracted from all the previous images acquired for that particular bouton to obtain releasable fluorescence values. The releasable fluorescence of each bouton during the stimulation is represented as a percentage of the average fluorescence of that bouton prior to stimulation. Typically, 20–100 boutons were analyzed per cover slip.

Whole-cell recordings in cultured neurons

Primary hippocampal neurons (DIV10–12) cultured on glass cover slips were used for tight seal conventional whole cell recordings. Cover slips were placed in a recording chamber with bath solution containing (in mM): 119 NaCl, 5 KCl, 20 HEPES, 30 glucose, 2 $CaCl_2$, 2 $MgCl_2$ and (in μM): 100 picrotoxin, 1 glycine, and 1 TTX. The pH and osmolarity of the bath solution were adjusted to 7.3 and 330 mOsm/L, respectively. Glass pipettes were filled with intracellular electrode solution (pH 7.3, 285 mOsm/L) containing (in mM): 130 K-gluconate, 10 KCl, 10 HEPES, 1 $MgCl_2$, 0.06 $CaCl_2$, 0.1 EGTA, 4 MgATP, 0.3 Na_2GTP, and 10 phosphocreatine and typically registered 5–7 MΩ pipette resistances. Recordings were performed at room temperature under constant perfusion (2 mL/minute) and acquired using Clampex software and a microamplifier (MultiClamp 700B, Molecular Devices). For mEPSCs measurements, cells were recorded at −70mV for 10 minutes. For measuring AMPA responses, responses at different holding membrane potentials were measured following a puff application (5 psi) (Picospritzer II) of 100 μM AMPA via a patch pipette located 100μm from the patched soma. A 5mV hyperpolarizing test pulse was applied

periodically during recordings to ensure that the access resistance did not change significantly and was less than 25MΩ. If so, the recordings were discarded. Signals were filtered at 2 kHz, digitized at 10 kHz, stored and analyzed off-line using MiniAnalysis Software (Synaptosoft Version 6.0.7) and Clampfit 10 (Molecular Devices). For miniature events analysis, the threshold for event detection was set at 5pA.

Whole-cell recordings in acute hippocampal slices

Coronal brain sections (350 μm) from juvenile mice (P14–17) were prepared using a vibratome (Leica VT1000S) in cold 95% O_2 / 5% CO_2-bubbled sucrose based solution (pH 7.4, 310 mOsm/L) containing (in mM): 195 sucrose, 10 NaCl, 25 $NaHCO_3$, 10 glucose, 2.5 KCl, 1.25 NaH_2PO_4, 2 Na-pyruvate, 0.5 $CaCl_2$, and 7 $MgCl_2$. Prior to recording, slices were recovered at room temperature in ACSF containing (in mM): 125 NaCl, 25 glucose, 25 $NaHCO_3$, 2.5 KCl, 1.25 NaH_2PO_4, 2 $CaCl_2$, and 1 $MgCl_2$ (pH 7.4, 300 mOsm/L). For measurements, slices were transferred to a recording chamber under constant perfusion (1 mL/minute) of 95% O_2 / 5% CO_2-bubbled artificial cerebrospinal fluid (ACSF). Patch pipettes were filled with a solution (pH 7.3, 285mOsm/L) containing (in mM): 117.5 Cs_2MeSO_4, 17.5 CsCl, 10 Hepes, 4 NaCl, 1 EGTA, 4 MgATP, 0.3 Na_2GTP, 10 phosphocreatine-Tris, and 10 QX-314Cl and typically registered pipette resistances of 5–7 MΩ. For rectification index measurements, spermine was added to the patch pipette. CA1 pyramidal cells were selected by morphology and patched using infrared DIC video microscopy. Following acquisition of electrical access, cells were held in voltage-clamp mode at −70mV for at least 10 minutes to ensure complete dialysis of the cell with the pipette solution. EPSCs were evoked by stimulation of Schaffer collateral fibers using a concentric bipolar stimulating electrode (0.25 ms) with a stimulator (S48, Grass Instruments) and stimulator isolation unit (SIU 5). EPSCs were recorded at different holding potentials. The EPSCs were quantified as the peak current minus baseline current prior to stimulation.

Protein extraction from hippocampal tissue

Hippocampi from individual P14 mice were individually transferred to 2 mLs of solubilization buffer containing (in mM): 10 HEPES, 320 sucrose, 1 EDTA, pH 7.4, and 1x cocktail of protease inhibitors (Thermo Scientific). The tissue was homogenized by Dounce homogenization and the homogenate spun at 1000g for 15′ at 4 C. The S1 fraction was retained and spun at 25,000g for 30′ at 4°C. The P2 pellet was re-suspended in 100μL of RIPA buffer containing 1% Triton X-100. 10μL of the solubilized P2 protein extract was removed for protein estimation and 2x loading buffer was added to the remaining lysate. Protein samples were vortexed, heated at 95 C, separated by SDS-PAGE, and blotted onto nitrocellulose membrane. Standard immunoblot technique was performed to probe for GluA1–4, phosphorylated GluA1, and tubulin proteins. Immunoreactive bands were quantified using ImageJ software.

Extracellular field recordings

Brains were quickly removed from P14–17 mice killed by cervical dislocation and placed in cold ACSF (bubbled with 95% O_2 / 5% CO_2) containing (in mM): 124 NaCl, 4 KCl, 1 Na_2HPO_4, 25 $NaHCO_3$, 2 $CaCl_2$, 2 $MgCl_2$, and 10 glucose. The pH and osmolarity of the solution was 7.4 and 310 mOsm/L, respectively. The hippocampus was isolated by dissection and placed on a mechanical tissue chopper to produce transverse hippocampal slices of 400μm thickness. Slices were maintained in a humidified interface chamber at 29°C and continuously perfused (~ 1mL/minute) with 95% O_2 / 5% CO_2-bubbled ACSF. Hippocampal slices were allowed to recover for at least 90 minutes prior to recording. For recordings, glass electrodes were filled with ACSF and positioned in the CA1 *stratum*

radiatum to record fEPSPs evoked by local stimulation (0.1ms) of Schaffer collateral fibers using a bipolar concentric microelectrode placed laterally to the recording electrode (~ 150 μm). Extracellular responses were acquired using Clampex software and a microamplifier (IE-210, Warner Instruments). For evaluating basal fEPSPs and fiber volleys, input-output curves were generated by plotting the slope (10–90%) of the fEPSP and the amplitude of the fiber volley as a function of the intensity of the voltage stimulation (5–15V).

For PPF and LTP recordings, the voltage intensity of the stimulation test pulse for each slice was determined to be the voltage intensity that had generated of the maximum slope obtained using input-output relationships. For PPF, Schaffer collaterals were stimulated with two pulses of varying inter-pulse durations (10, 20, 30, 40, 50, 100, 200, 300, 400, 500, and 1000 ms). Facilitation was calculated as the ratio of the slopes of the second and first fEPSPs, and plotted as a function of the inter-pulse duration. For LTP, a test pulse was applied every minute. Following a steady baseline of at least 10 minutes, LTP was induced with a theta-burst stimulation (TBS) involving a single train of ten bursts at 5Hz, where each burst is composed of 4 pulses at 100Hz. For a triple TBS stimulation, three sequential trains of bursts was applied at 15s intervals. The fEPSP slopes following tetanic stimulation were normalized to the average of the slopes of the fEPSPs acquired during the baseline. Potentiation one hour post-tetanus was calculated by averaging the fEPSP slopes occurring over the last five minutes of the recording.

Statistics

The Mann Whitney test (Prism, GraphPad) for nonparametric data was used to test for statistical significance between +/+ and sdy/sdy genotypes. For quantal analysis, differences in the frequency and amplitude of mEPSCs were evaluated between recorded cells of each genotype. For FM dye analysis, differences between tau values for individual experiments were evaluated between coverslips of each genotype. For immunoblot analysis, differences in immunoreactive values of protein levels normalized to tubulin were evaluated between individual animals of each genotype. For current voltage relations, differences in current were evaluated between cells of each genotype. For PPF measurements, values measured at all inter-stimulus times were evaluated between slices of each genotype. For parametric data, Two-Way ANOVA was used to evaluate input-output relations for fEPSP slopes between slices of each genotype for stimulation intensities from 5–15V. Two-Way ANOVA was used to evaluate LTP recordings between slices of each genotype for all normalized fEPSP values measured after the tetanus application. Statistical significance was assigned for p values less than 0.05.

Results

Dysbindin affects AMPAR responses in hippocampal cultures

We first looked for changes in neurotransmission in hippocampal cultures from homozygous mutant mice for the sandy allele (sdy/sdy) and wild-type control littermates (+/+). Whole cell voltage-clamp measurements were obtained from cultured hippocampal neurons for quantal analysis. The average frequency of miniature excitatory post-synaptic currents (mEPSCs), a measure of pre-synaptic function, was not significantly different between +/+ and sdy/sdy neurons (+/+: 251 ± 67 events/min versus sdy/sdy: 231 ± 46 events/min; Figure 1A). To further examine whether dysbindin affects the probability of evoked synaptic vesicle exocytosis, we employed FM dye analysis of cultured neurons to measure the de-staining rate of boutons labeled with FM 4–64 by electrical stimulation (Figure 1B). The rate of fluorescence decrease of labeled boutons, which reflects synaptic vesicle exocytosis (Ryan et al., 1996; Ryan and Smith, 1995), was comparable between +/+ and sdy/sdy cells using a field stimulation of 10Hz suggesting that loss of dysbindin expression did not alter

the rate of synaptic vesicle exocytosis (+/+: $\tau = 14 \pm 5$ versus sdy/sdy: $\tau = 21 \pm 5$; Figure 1B).

A significant enhancement in the amplitude of mEPSCs between +/+ and sdy/sdy cells (+/+: 9.7 ± 0.7 pA versus sdy/sdy: 13.4 ± 1.7 pA, $p<0.05$, Figure 1A) was observed suggesting that the loss of dysbindin led to an increase in post-synaptic responsiveness. To validate this finding, AMPA was applied locally onto voltage-clamped cells by pressure application to evaluate current-voltage relations in sdy/sdy compared to +/+ neurons. We found that the peak current of AMPA responses was significantly enhanced in sdy/sdy compared to +/+ neurons (At V_h: −70mV| +/+: 267 ± 73 pA versus sdy/sdy: 548 ± 89 pA, $p<0.05$, Figure 1C). Altogether, these results revealed that dysbindin modulates AMPAR responses in hippocampal cultures.

Measurement of GluA subunit expression in juvenile hippocampal tissue

Due to the enhanced AMPAR function in cultured sdy/sdy hippocampal neurons, we examined the protein stability of individual GluA1–4 subunits that comprise the heterotetrameric AMPAR complex (Hollmann and Heinemann, 1994; Jensen et al., 2003; Rosenmund et al., 1998) in the hippocampus of juvenile aged +/+ and sdy/sdy littermates (P14). Immunoblot analysis revealed no changes in the total expression levels of GluA1–4 (Figure 2A). The expression levels of two phosphorylated GluA1 subunits, S831P, which is associated with increased single channel conductance (Derkach et al., 1999), and S845P, which is associated with increased surface insertion of GluA1P containing AMPAR complexes (Ehlers, 2000) were also unchanged in the sdy/sdy mice compared to +/+ controls (Figure 2B).

Dysbindin expression modulates CA3-CA1 AMPAR-mediated synaptic transmission

We proceeded to test whether changes in AMPAR current could be detected in acute brain slice prepared from sdy/sdy and +/+ mice. Using whole cell recordings in voltage-clamp mode, CA1 AMPAR mediated EPSCs evoked by stimulation of Schaffer-collateral inputs were measured. We found that the peak currents of EPSCs were significantly enhanced in sdy/sdy slices compared to +/+ littermates (V_h: −70mV| +/+: 267 ± 73 pA, sdy/sdy: 548 ± 89 pA, $p<0.05$, Figure 3A). The enhancement of CA1 AMPAR-mediated EPSCs was consistent with the enhancement of AMPA responses observed in hippocampal cultures (Figure 1A and 1C).

To test whether the enhanced CA1 AMPAR-mediated transmission in sdy/sdy mice was due to the enhanced insertion of GluR2-lacking calcium permeable AMPARs (Plant et al., 2006) we repeated measurements of evoked CA1 EPSCs with the addition of spermine in the patch pipette. Intracellular spermine affects the voltage-dependency of GluR2-lacking AMPARs by inhibiting currents at positive membrane holding potentials (Donevan and Rogawski, 1995). No changes in inward rectification were, however, found in sdy/sdy synapses compared to +/+ (Figure 3C). To test whether loss of dysbindin led to a general defect in post-synaptic receptor function, we also evaluated CA1 NMDAR-mediated synaptic transmission. The peak current of NMDAR-mediated EPSCs between sdy/sdy and +/+ synapses were comparable (at V_h: +60mV| +/+: 350 ± 54 pA, sdy/sdy: 462 ± 75 pA; See Figure 3C), suggesting that dysbindin specifically modulates AMPAR-mediated synaptic responses rather than causing a general defect in post-synaptic receptor function.

Dysbindin expression modulates LTP

Based on compelling evidence that dysbindin modulates AMPAR function, we hypothesized that dysbindin expression is important for modulating LTP, which is believed to be an electrophysiological model underlying spatial learning and memory processes (Lynch,

2004). AMPARs have been shown to contribute to the expression of CA3-CA1 LTP (Hayashi et al, Science 2000, Park et al, Science, 2004, Jensen 2003). Using extracellular field recording analysis from acute juvenile hippocampal slices, we first performed input-output relations to evaluate basal excitatory synaptic transmission. Local field excitatory post-synaptic potentials (EPSPs) in the CA1 *stratum radiatum* were evoked by stimulation of the Schaffer collateral pathway using varying stimulation intensities. Over a stimulation intensity range of 5–15V, we found a significant enhancement of the fEPSP slope in sdy/sdy compared to +/+ synapses (15V| +/+: 1.6 ± 0.1 mV/ms versus sdy/sdy 2.1 ± 0.2 mV/ms; Two-Way ANOVA by genotype: f [1,24] = 4.821, $p<0.05$ by genotype; See Figure 4A). Between +/+ and sdy/sdy synapses, there were no changes in the amplitude of the fiber volley which is due to the generation of action potentials in the Schaffer collaterals (15V| +/+: 1.1 ± 0.2mV versus sdy/sdy: 1.2 ± 0.2mV; Figure 4B). Moreover, there were no changes in paired-pulse facilitation, one measure of pre-synaptic function (Zucker 2002), between +/+ and sdy/sdy CA3-CA1 synapses (See Figure 4C). Thus the enhanced basal synaptic transmission is likely due to AMPAR function which is consistent with the enhanced CA1 AMPAR-mediated synaptic transmission (Figure 4A) and AMPAR responses in cultured hippocampal neurons (Figure 1C).

We next looked for changes in CA3-CA1 LTP between +/+ and sdy/sdy slices induced by tetanization of the Schaffer collateral pathway using a theta-burst stimulation (TBS) protocol. When a weak TBS protocol comprising a single train of bursts (4 pulses at 100Hz) repeated at 5Hz for 1s was applied, within 20 minutes significantly more potentiation could be observed in sdy/sdy compared to +/+ synapses. This enhanced LTP persisted for at least one hour (60 minutes post-tetanus | +/+: 114 ± 5%; sdy/sdy 153 ± 8%; f [1,13] = 10.51, $p<0.01$ by genotype; Figure 5A). To test whether loss of dysbindin affects the mechanisms of potentiation per se, rather than the intensity of the inducing stimulus, a strong TBS protocol comprising 3 trains of stimulation bursts separated by 15s was used. In WT slices, the strong protocol relative to the weak protocol led to higher levels of potentiation, while in sdy/sdy synapses, the strong protocol did not further enhance potentiation compared to the weaker protocol (+/+: 150 ± 5% versus sdy/sdy 168 ± 12%; See Figure 5B). These results suggest that loss of dysbindin did not increase the capacity of synapses for potentiation, but rather reduced the stimulation strength for generating a given amount of potentiation. Altogether, dysbindin expression appears to play an important role in controlling LTP at CA3-CA1 synapses.

Discussion

Using primarily an electrophysiological analysis of dysbindin-deficient hippocampal neurons in cultures and slices, we have uncovered a previously unreported role for dysbindin in enhancing CA3-CA1 AMPAR-mediated transmission. An earlier study, however, has reported a reduction in CA3-CA1 neurotransmission in the sandy mouse mutant attributed to a reduction in the probability of glutamate release (Chen et al., 2008). Furthermore, consistent with another study (Tang et al., 2009b), we found no changes in PPF, nor in mEPSC frequency, suggesting no changes in release probability. The disparity in results may be due to differences in the hippocampal sub-region studied. While their study investigated the ventral hippocampus, ours examined slices from dorsal and mid-septotemporal hippocampus. An interesting hypothesis is that loss of dysbindin expression could modulate synaptic transmission at either the pre- and post-synaptic locus depending on the anatomical location within the hippocampus. Fractionation of purified hippocampal synapses has indeed revealed that dysbindin is present in both pre- and post-synaptic compartments (Talbot et al., 2004; Talbot et al., 2011).

Similar to our findings, another group has also reported an enhancement of both CA3-CA1 glutamatergic transmission and LTP in the sandy mutant. However, in contrast with our study, these effects were attributed to enhanced surface expression of NR2A-containing NMDA receptors (Tang et al., 2009b). Thus, it remains unclear why dysbindin affected NMDAR function in their study and AMPAR function in ours, but could be due to the different genetic background strains used, C57Bl/6J and DBA/2J, respectively. It has indeed been found that strain background strongly affects the phenotype in the sandy mouse which can lead to behavioral defects in the opposite direction (Cox et al., 2009; Hattori et al., 2008; Ji et al., 2009; Takao et al., 2008).

We report compelling evidence that dysbindin modulates AMPAR-mediated transmission. The precise mechanism of such modulation remains undefined. Dysbindin has been found in the nucleus and appears to affect gene transcription (Fei et al., 2010). However, we found no changes in the hippocampal expression levels of GluA1–4. Studies have shown that loss or reduced dysbindin expression lead to an increase in the surface expression of the NR2A-containing NMDA receptor and the D2R due to protein mis-trafficking (Iizuka et al., 2007; Ji et al., 2009; Marley and von Zastrow, 2010; Tang et al., 2009b). Moreover, a mutation in the DTNBP1 gene leads to Hermansky-Pudlak syndrome in humans, characterized by defects in blood clotting and pigmentation (Li et al., 2003). This is due to defects in a specialized class of lysosome-related organelles, important for the storage of molecules to be secreted (Di Pietro and Dell'Angelica, 2005; Di Pietro et al., 2006). Therefore, one mechanism for the enhanced AMPAR response seen here may involve the mis-trafficking of AMPARs from intracellular endosomal stores (Lee et al., 2001) to the membrane surface of synapses (Park et al., 2004). Several studies have found that dysbindin interacts with components of the exocyst complex (Camargo et al., 2007; Gokhale et al., 2012; Mead et al., 2010) which has been shown to be involved in the trafficking of the AMPAR to the membrane surface (Gerges et al., 2006; Mao et al., 2010). An alternative functional partner may involve another susceptibility gene for schizophrenia, Disrupted in schizophrenia (DISC) 1 (St Clair et al., 1990). It was reported that a reduction of DISC1 led to an increase in surface expression of GluR1 (Wang et al., 2011). An interaction between dysbindin and DISC1 has been reported (Ottis et al., 2011) suggesting that these two could modulate AMPAR trafficking through a common mechanism.

Because of dysbindin's link to schizophrenia, our data points to a potential role for AMPAR-mediated synaptic transmission in the disorder. Post-mortem studies of schizophrenia patients have generally found a reduction of AMPARs in the hippocampus (Kerwin et al., 1990). However, analysis of schizophrenia patient brain tissue revealed an increase of GluA1 in early endosomes, and an increase in the expression of GRIP1 and SAP97, two proteins involved in AMPAR trafficking, as well as changes in the expression of regulatory proteins of AMPAR function (Drummond et al., 2013; Hammond et al., 2010). Based on these data, the authors concluded that an abnormality in forward trafficking of AMPARs to the synapse was associated with the disease pathophysiology. Further evidence for a role of AMPAR in schizophrenia can be seen in a mouse model which does not express GluA1 subunit and displays behavioral phenotypes related to schizophrenia (Wiedholz et al., 2008). Based on these studies it appears that proper modulation of AMPAR-mediated synaptic transmission by dysbindin is an integral component in the prevention of schizophrenia.

In light of several reports of defects in memory-related tasks for the dysbindin-deficient mice (Cox et al., 2009; Takao et al., 2008), it was rather unexpected that an enhancement of CA3-CA1 LTP was observed in our investigation as well as in another independent study (Tang et al., 2009b). The relationship between LTP and learning and memory is, however, not always strictly correlative since several mice mutants with enhanced LTP display

impairments in memory-related behavior (Meng et al., 2002; Migaud et al., 1998; Uetani et al., 2000). Clinical features of schizophrenia include the positive symptoms of psychosis involving hallucinations and delusions. An association between a DTNBP1 gene variant and early-onset psychosis has been reported (Fatjo-Vilas et al., 2011). It was theorized that psychosis could be mediated by the inappropriate encoding of memories due to a mechanism involving enhanced synaptic transmission along an altered hippocampal excitatory pathway (Tamminga et al., 2010). Based on the data described here, we propose that loss of dysbindin may contribute to inappropriate memory encoding by alterations in AMPAR-mediated transmission and plasticity.

Conclusions

We report a novel role for dysbindin expression in modulating post-synaptic AMPAR function in juvenile DBA/2J mice. These results are consistent with an emerging role for dysbindin in modulating receptor function in the brain. The mechanism for how this occurs remains an open question for further investigation. Moreover, this study implies that proper AMPA receptor transmission and plasticity during juvenile brain development may play an important role in the pathophysiology of schizophrenia.

Acknowledgments

We thank Dr. R Swank for acquisition of the sandy mice and to Dr. L Role, Dr. D Sulzer, Dr. G DiPaolo, Dr. A Yamamoto and fellow lab members for their critical input during the entire course of this study. Part of this work was presented in a poster at the 2010 Society for Neuroscience Meeting. This work was financed by grants from the National Institute of Health awarded to OA (NIH-NS049442) and a pre-doctoral NRSA training fellowship awarded to IO.

Abbreviations

AMPAR	2-amino-3-(3-hydroxy-5-methyl-isoxazol-4-yl) propanoic acid receptor
NMDAR	*N*-Methyl-D-aspartic acid receptor
LTP	Long-term potentiation

References

Camargo LM, Collura V, Rain JC, Mizuguchi K, Hermjakob H, Kerrien S, Bonnert TP, Whiting PJ, Brandon NJ. Disrupted in Schizophrenia 1 Interactome: evidence for the close connectivity of risk genes and a potential synaptic basis for schizophrenia. Mol Psychiatry. 2007; 12:74–86. [PubMed: 17043677]

Chen XW, Feng YQ, Hao CJ, Guo XL, He X, Zhou ZY, Guo N, Huang HP, Xiong W, Zheng H, Zuo PL, Zhang CX, Li W, Zhou Z. DTNBP1, a schizophrenia susceptibility gene, affects kinetics of transmitter release. The Journal of cell biology. 2008; 181:791–801. [PubMed: 18504299]

Cox MM, Tucker AM, Tang J, Talbot K, Richer DC, Yeh L, Arnold SE. Neurobehavioral abnormalities in the dysbindin-1 mutant, sandy, on a C57BL/6J genetic background. Genes Brain Behav. 2009; 8:390–397. [PubMed: 19220483]

Derkach V, Barria A, Soderling TR. Ca2+/calmodulin-kinase II enhances channel conductance of alpha-amino-3-hydroxy-5-methyl-4-isoxazolepropionate type glutamate receptors. Proc Natl Acad Sci U S A. 1999; 96:3269–3274. [PubMed: 10077673]

Di Pietro SM, Dell'Angelica EC. The cell biology of Hermansky-Pudlak syndrome: recent advances. Traffic. 2005; 6:525–533. [PubMed: 15941404]

Di Pietro SM, Falcon-Perez JM, Tenza D, Setty SR, Marks MS, Raposo G, Dell'Angelica EC. BLOC-1 interacts with BLOC-2 and the AP-3 complex to facilitate protein trafficking on endosomes. Molecular biology of the cell. 2006; 17:4027–4038. [PubMed: 16837549]

Donevan SD, Rogawski MA. Intracellular polyamines mediate inward rectification of Ca(2+)-permeable alpha-amino-3-hydroxy-5-methyl-4-isoxazolepropionic acid receptors. Proc Natl Acad Sci U S A. 1995; 92:9298–9302. [PubMed: 7568121]

Drummond JB, Tucholski J, Haroutunian V, Meador-Woodruff JH. Transmembrane AMPA receptor regulatory protein (TARP) dysregulation in anterior cingulate cortex in schizophrenia. Schizophr Res. 2013

Ehlers MD. Reinsertion or degradation of AMPA receptors determined by activity-dependent endocytic sorting. Neuron. 2000; 28:511–525. [PubMed: 11144360]

Fatjo-Vilas M, Papiol S, Estrada G, Bombin I, Peralta V, Rosa A, Parellada M, Miret S, Martin M, Lazaro L, Campanera S, Munoz MJ, Lera-Miguel S, Arias B, Navarro ME, Castro-Fornieles J, Cuesta MJ, Arango C, Fananas L. Dysbindin-1 gene contributes differentially to early- and adult-onset forms of functional psychosis. Am J Med Genet B Neuropsychiatr Genet. 2011; 156:322–333. [PubMed: 21305691]

Fei E, Ma X, Zhu C, Xue T, Yan J, Xu Y, Zhou J, Wang G. Nucleocytoplasmic shuttling of dysbindin-1, a schizophrenia-related protein, regulates synapsin I expression. J Biol Chem. 2010; 285:38630–38640. [PubMed: 20921223]

Gerges NZ, Backos DS, Rupasinghe CN, Spaller MR, Esteban JA. Dual role of the exocyst in AMPA receptor targeting and insertion into the postsynaptic membrane. EMBO J. 2006; 25:1623–1634. [PubMed: 16601687]

Ghiani CA, Starcevic M, Rodriguez-Fernandez IA, Nazarian R, Cheli VT, Chan LN, Malvar JS, de Vellis J, Sabatti C, Dell'Angelica EC. The dysbindin-containing complex (BLOC-1) in brain: developmental regulation, interaction with SNARE proteins and role in neurite outgrowth. Mol Psychiatry. 2010; 15:115, 204–115. [PubMed: 19546860]

Gokhale A, Larimore J, Werner E, So L, Moreno-De-Luca A, Lese-Martin C, Lupashin VV, Smith Y, Faundez V. Quantitative proteomic and genetic analyses of the schizophrenia susceptibility factor dysbindin identify novel roles of the biogenesis of lysosome-related organelles complex 1. The Journal of neuroscience: the official journal of the Society for Neuroscience. 2012; 32:3697–3711. [PubMed: 22423091]

Hammond JC, McCullumsmith RE, Funk AJ, Haroutunian V, Meador-Woodruff JH. Evidence for abnormal forward trafficking of AMPA receptors in frontal cortex of elderly patients with schizophrenia. Neuropsychopharmacology. 2010; 35:2110–2119. [PubMed: 20571483]

Hattori S, Murotani T, Matsuzaki S, Ishizuka T, Kumamoto N, Takeda M, Tohyama M, Yamatodani A, Kunugi H, Hashimoto R. Behavioral abnormalities and dopamine reductions in sdy mutant mice with a deletion in Dtnbp1, a susceptibility gene for schizophrenia. Biochem Biophys Res Commun. 2008; 373:298–302. [PubMed: 18555792]

Hikita T, Taya S, Fujino Y, Taneichi-Kuroda S, Ohta K, Tsuboi D, Shinoda T, Kuroda K, Funahashi Y, Uraguchi-Asaki J, Hashimoto R, Kaibuchi K. Proteomic analysis reveals novel binding partners of dysbindin, a schizophrenia-related protein. J Neurochem. 2009; 110:1567–1574. [PubMed: 19573021]

Hollmann M, Heinemann S. Cloned glutamate receptors. Annu Rev Neurosci. 1994; 17:31–108. [PubMed: 8210177]

Iizuka Y, Sei Y, Weinberger DR, Straub RE. Evidence that the BLOC-1 protein dysbindin modulates dopamine D2 receptor internalization and signaling but not D1 internalization. The Journal of neuroscience: the official journal of the Society for Neuroscience. 2007; 27:12390–12395. [PubMed: 17989303]

Ito H, Morishita R, Shinoda T, Iwamoto I, Sudo K, Okamoto K, Nagata K. Dysbindin-1, WAVE2 and Abi-1 form a complex that regulates dendritic spine formation. Mol Psychiatry. 2010; 15:976–986. [PubMed: 20531346]

Jensen V, Kaiser KM, Borchardt T, Adelmann G, Rozov A, Burnashev N, Brix C, Frotscher M, Andersen P, Hvalby O, Sakmann B, Seeburg PH, Sprengel R. A juvenile form of postsynaptic hippocampal long-term potentiation in mice deficient for the AMPA receptor subunit GluR-A. J Physiol. 2003; 553:843–856. [PubMed: 14555717]

Ji Y, Yang F, Papaleo F, Wang HX, Gao WJ, Weinberger DR, Lu B. Role of dysbindin in dopamine receptor trafficking and cortical GABA function. Proc Natl Acad Sci U S A. 2009; 106:19593–19598. [PubMed: 19887632]

Kerwin R, Patel S, Meldrum B. Quantitative autoradiographic analysis of glutamate binding sites in the hippocampal formation in normal and schizophrenic brain post mortem. Neuroscience. 1990; 39:25–32. [PubMed: 1982465]

Kubota K, Kumamoto N, Matsuzaki S, Hashimoto R, Hattori T, Okuda H, Takamura H, Takeda M, Katayama T, Tohyama M. Dysbindin engages in c-Jun N-terminal kinase activity and cytoskeletal organization. Biochem Biophys Res Commun. 2009; 379:191–195. [PubMed: 19094965]

Larimore J, Tornieri K, Ryder PV, Gokhale A, Zlatic SA, Craige B, Lee JD, Talbot K, Pare JF, Smith Y, Faundez V. The schizophrenia susceptibility factor dysbindin and its associated complex sort cargoes from cell bodies to the synapse. Molecular biology of the cell. 2011; 22:4854–4867. [PubMed: 21998198]

Lee SH, Valtschanoff JG, Kharazia VN, Weinberg R, Sheng M. Biochemical and morphological characterization of an intracellular membrane compartment containing AMPA receptors. Neuropharmacology. 2001; 41:680–692. [PubMed: 11640922]

Li W, Zhang Q, Oiso N, Novak EK, Gautam R, O'Brien EP, Tinsley CL, Blake DJ, Spritz RA, Copeland NG, Jenkins NA, Amato D, Roe BA, Starcevic M, Dell'Angelica EC, Elliott RW, Mishra V, Kingsmore SF, Paylor RE, Swank RT. Hermansky-Pudlak syndrome type 7 (HPS-7) results from mutant dysbindin, a member of the biogenesis of lysosome-related organelles complex 1 (BLOC-1). Nature genetics. 2003; 35:84–89. [PubMed: 12923531]

Lutkenhoff E, Karlsgodt KH, Gutman B, Stein JL, Thompson PM, Cannon TD, Jentsch JD. Structural and functional neuroimaging phenotypes in dysbindin mutant mice. Neuroimage. 2012; 62:120–129. [PubMed: 22584233]

Lynch MA. Long-term potentiation and memory. Physiol Rev. 2004; 84:87–136. [PubMed: 14715912]

Ma X, Fei E, Fu C, Ren H, Wang G. Dysbindin-1, a schizophrenia-related protein, facilitates neurite outgrowth by promoting the transcriptional activity of p53. Mol Psychiatry. 2011

Mao L, Takamiya K, Thomas G, Lin DT, Huganir RL. GRIP1 and 2 regulate activity-dependent AMPA receptor recycling via exocyst complex interactions. Proc Natl Acad Sci U S A. 2010; 107:19038–19043. [PubMed: 20956289]

Marley A, von Zastrow M. Dysbindin promotes the post-endocytic sorting of G protein-coupled receptors to lysosomes. PLoS One. 2010; 5:e9325. [PubMed: 20174469]

Mead CL, Kuzyk MA, Moradian A, Wilson GM, Holt RA, Morin GB. Cytosolic protein interactions of the schizophrenia susceptibility gene dysbindin. J Neurochem. 2010; 113:1491–1503. [PubMed: 20236384]

Mechelli A, Viding E, Kumar A, Pettersson-Yeo W, Fusar-Poli P, Tognin S, O'Donovan MC, McGuire P. Dysbindin modulates brain function during visual processing in children. Neuroimage. 2010; 49:817–822. [PubMed: 19631276]

Meng Y, Zhang Y, Tregoubov V, Janus C, Cruz L, Jackson M, Lu WY, MacDonald JF, Wang JY, Falls DL, Jia Z. Abnormal spine morphology and enhanced LTP in LIMK-1 knockout mice. Neuron. 2002; 35:121–133. [PubMed: 12123613]

Migaud M, Charlesworth P, Dempster M, Webster LC, Watabe AM, Makhinson M, He Y, Ramsay MF, Morris RG, Morrison JH, O'Dell TJ, Grant SG. Enhanced long-term potentiation and impaired learning in mice with mutant postsynaptic density-95 protein. Nature. 1998; 396:433–439. [PubMed: 9853749]

Ottis P, Bader V, Trossbach SV, Kretzschmar H, Michel M, Leliveld SR, Korth C. Convergence of two independent mental disease genes on the protein level: recruitment of dysbindin to cell-invasive disrupted-in-schizophrenia 1 aggresomes. Biol Psychiatry. 2011; 70:604–610. [PubMed: 21531389]

Park M, Penick EC, Edwards JG, Kauer JA, Ehlers MD. Recycling endosomes supply AMPA receptors for LTP. Science. 2004; 305:1972–1975. [PubMed: 15448273]

Plant K, Pelkey KA, Bortolotto ZA, Morita D, Terashima A, McBain CJ, Collingridge GL, Isaac JT. Transient incorporation of native GluR2-lacking AMPA receptors during hippocampal long-term potentiation. Nat Neurosci. 2006; 9:602–604. [PubMed: 16582904]

Rapoport JL, Addington AM, Frangou S, Psych MR. The neurodevelopmental model of schizophrenia: update 2005. Mol Psychiatry. 2005; 10:434–449. [PubMed: 15700048]

Rosenmund C, Stern-Bach Y, Stevens CF. The tetrameric structure of a glutamate receptor channel. Science. 1998; 280:1596–1599. [PubMed: 9616121]

Ryan TA, Li L, Chin LS, Greengard P, Smith SJ. Synaptic vesicle recycling in synapsin I knockout mice. The Journal of cell biology. 1996; 134:1219–1227. [PubMed: 8794863]

Ryan TA, Smith SJ. Vesicle pool mobilization during action potential firing at hippocampal synapses. Neuron. 1995; 14:983–989. [PubMed: 7748565]

St Clair D, Blackwood D, Muir W, Carothers A, Walker M, Spowart G, Gosden C, Evans HJ. Association within a family of a balanced autosomal translocation with major mental illness. Lancet. 1990; 336:13–16. [PubMed: 1973210]

Starcevic M, Dell'Angelica EC. Identification of snapin and three novel proteins (BLOS1, BLOS2, and BLOS3/reduced pigmentation) as subunits of biogenesis of lysosome-related organelles complex-1 (BLOC-1). J Biol Chem. 2004; 279:28393–28401. [PubMed: 15102850]

Straub RE, Jiang Y, MacLean CJ, Ma Y, Webb BT, Myakishev MV, Harris-Kerr C, Wormley B, Sadek H, Kadambi B, Cesare AJ, Gibberman A, Wang X, O'Neill FA, Walsh D, Kendler KS. Genetic variation in the 6p22.3 gene DTNBP1, the human ortholog of the mouse dysbindin gene, is associated with schizophrenia. Am J Hum Genet. 2002; 71:337–348. [PubMed: 12098102]

Takao K, Toyama K, Nakanishi K, Hattori S, Takamura H, Takeda M, Miyakawa T, Hashimoto R. Impaired long-term memory retention and working memory in sdy mutant mice with a deletion in Dtnbp1, a susceptibility gene for schizophrenia. Mol Brain. 2008; 1:11. [PubMed: 18945333]

Talbot K, Eidem WL, Tinsley CL, Benson MA, Thompson EW, Smith RJ, Hahn CG, Siegel SJ, Trojanowski JQ, Gur RE, Blake DJ, Arnold SE. Dysbindin-1 is reduced in intrinsic, glutamatergic terminals of the hippocampal formation in schizophrenia. The Journal of clinical investigation. 2004; 113:1353–1363. [PubMed: 15124027]

Talbot K, Louneva N, Cohen JW, Kazi H, Blake DJ, Arnold SE. Synaptic dysbindin-1 reductions in schizophrenia occur in an isoform-specific manner indicating their subsynaptic location. PLoS One. 2011; 6:e16886. [PubMed: 21390302]

Tamminga CA, Stan AD, Wagner AD. The hippocampal formation in schizophrenia. Am J Psychiatry. 2010; 167:1178–1193. [PubMed: 20810471]

Taneichi-Kuroda S, Taya S, Hikita T, Fujino Y, Kaibuchi K. Direct interaction of Dysbindin with the AP-3 complex via its mu subunit. Neurochem Int. 2009; 54:431–438. [PubMed: 19428785]

Tang J, LeGros RP, Louneva N, Yeh L, Cohen JW, Hahn CG, Blake DJ, Arnold SE, Talbot K. Dysbindin-1 in dorsolateral prefrontal cortex of schizophrenia cases is reduced in an isoform-specific manner unrelated to dysbindin-1 mRNA expression. Hum Mol Genet. 2009a; 18:3851–3863. [PubMed: 19617633]

Tang TT, Yang F, Chen BS, Lu Y, Ji Y, Roche KW, Lu B. Dysbindin regulates hippocampal LTP by controlling NMDA receptor surface expression. Proc Natl Acad Sci U S A. 2009b; 106:21395–21400. [PubMed: 19955431]

Tognin S, Viding E, McCrory EJ, Taylor L, O'Donovan MC, McGuire P, Mechelli A. Effects of DTNBP1 genotype on brain development in children. J Child Psychol Psychiatry. 2011

Uetani N, Kato K, Ogura H, Mizuno K, Kawano K, Mikoshiba K, Yakura H, Asano M, Iwakura Y. Impaired learning with enhanced hippocampal long-term potentiation in PTPdelta-deficient mice. EMBO J. 2000; 19:2775–2785. [PubMed: 10856223]

Wang Q, Charych EI, Pulito VL, Lee JB, Graziane NM, Crozier RA, Revilla-Sanchez R, Kelly MP, Dunlop AJ, Murdoch H, Taylor N, Xie Y, Pausch M, Hayashi-Takagi A, Ishizuka K, Seshadri S, Bates B, Kariya K, Sawa A, Weinberg RJ, Moss SJ, Houslay MD, Yan Z, Brandon NJ. The psychiatric disease risk factors DISC1 and TNIK interact to regulate synapse composition and function. Mol Psychiatry. 2011; 16:1006–1023. [PubMed: 20838393]

Weickert CS, Rothmond DA, Hyde TM, Kleinman JE, Straub RE. Reduced DTNBP1 (dysbindin-1) mRNA in the hippocampal formation of schizophrenia patients. Schizophr Res. 2008; 98:105–110. [PubMed: 17961984]

Wiedholz LM, Owens WA, Horton RE, Feyder M, Karlsson RM, Hefner K, Sprengel R, Celikel T, Daws LC, Holmes A. Mice lacking the AMPA GluR1 receptor exhibit striatal hyperdopaminergia and 'schizophrenia-related' behaviors. Mol Psychiatry. 2008; 13:631–640. [PubMed: 17684498]

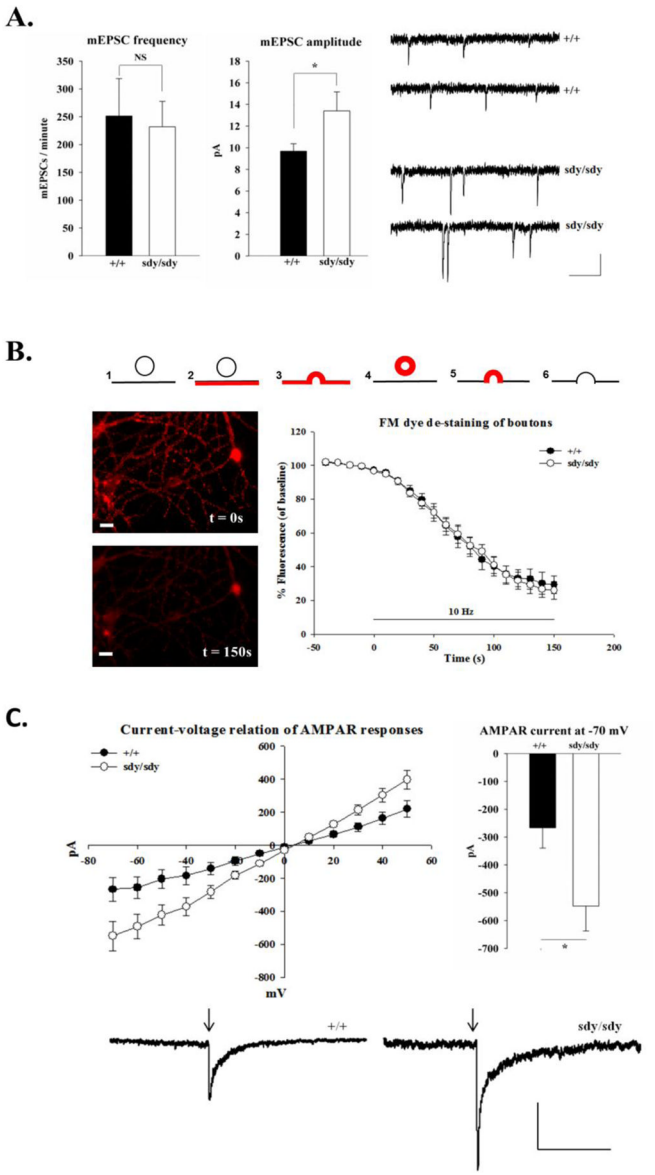

Figure 1. Enhanced AMPAR response in cultured sdy/sdy hippocampal neurons

A. The average frequency and amplitude of mEPSCs were measured from +/+ (n=15 cells) and sdy/sdy (n=11 cells) hippocampal neurons in culture (DIV 10–12) (See text for values). Sample traces are shown. Scale bars are 10 pA and 200 ms. Currents were measured from a holding potential of −70 mV with 1 μM TTX and 100 μM picrotoxin present in the bath solution. Measurements were taken 3 minutes after obtaining a stable whole-cell recording configuration. B. Cartoon describing the FM dye de-staining assay (upper panel): 1. Synaptic vesicles before dye addition. 2. Addition of 15 μM FM4–64 to cells. 3. Stimulation with 600 1ms pulses (10Hz, 60s) to load synaptic vesicles. 4. Washout excess dye with HEPES buffered sodium chloride solution. 5. Stimulate to unload vesicles (10Hz, 60s). 6. Destained vesicles. Representative images of stained (t = 0s) and de-stained (t = 150s) boutons from +/+ hippocampal cultures are shown. Scale bar is 10 μm. The percentage fluorescence (of baseline) was plotted as a function of time for measurements from +/+ (n = 292 boutons, 3 experiments) and sdy/sdy (n = 272 boutons, 3 experiments) cells. Baseline fluorescence represents the average fluorescence before stimulation. Decay rates were fit to

a single exponential equation. Time (t) = 0 represents the onset of stimulation. C. Somatic whole cell voltage clamp currents were measured from +/+ (n = 10 cells) and sdy/sdy (n = 10 cells) hippocampal cultures (DIV10–12) in response to 50 ms puffs (indicated by downward arrow) of 100 μM AMPA via a glass pipette. The puffs were applied at different holding potentials to generate current voltage relations. The bar graph shows the average peak amplitude of AMPA responses at V_h: −70 mV. Scale bars represent 100 pA and 1 s. Reported values represent mean ± SEM. Statistical analysis was performed using the Mann-Whitney test. An asterisk denotes $p<0.05$ while NS denotes data were not significant.

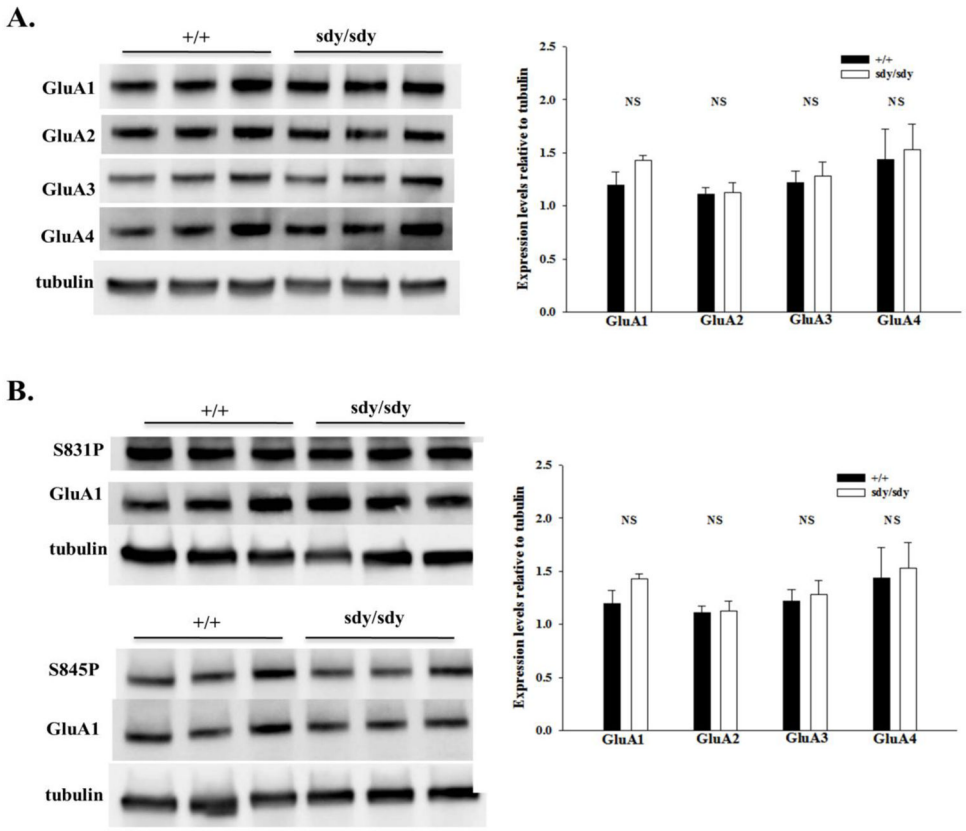

Figure 2. Expression levels of GluA1–4 and phosphorylated GluA1 subunits in sandy hippocampus

A. Immunoblot and quantification of immunoreactivity of GluA1–4 subunits in hippocampal P2 lysates from P14 +/+ and −/− mice. Tubulin was used as a loading control and for normalization. Hippocampi from three +/+ and three sdy/sdy mice were used for analysis. Approximately 25 μg of protein was loaded per lane. Reported values represent mean ± SEM. Statistical analysis was performed using the Mann-Whitney test. NS signifies $p>0.05$.

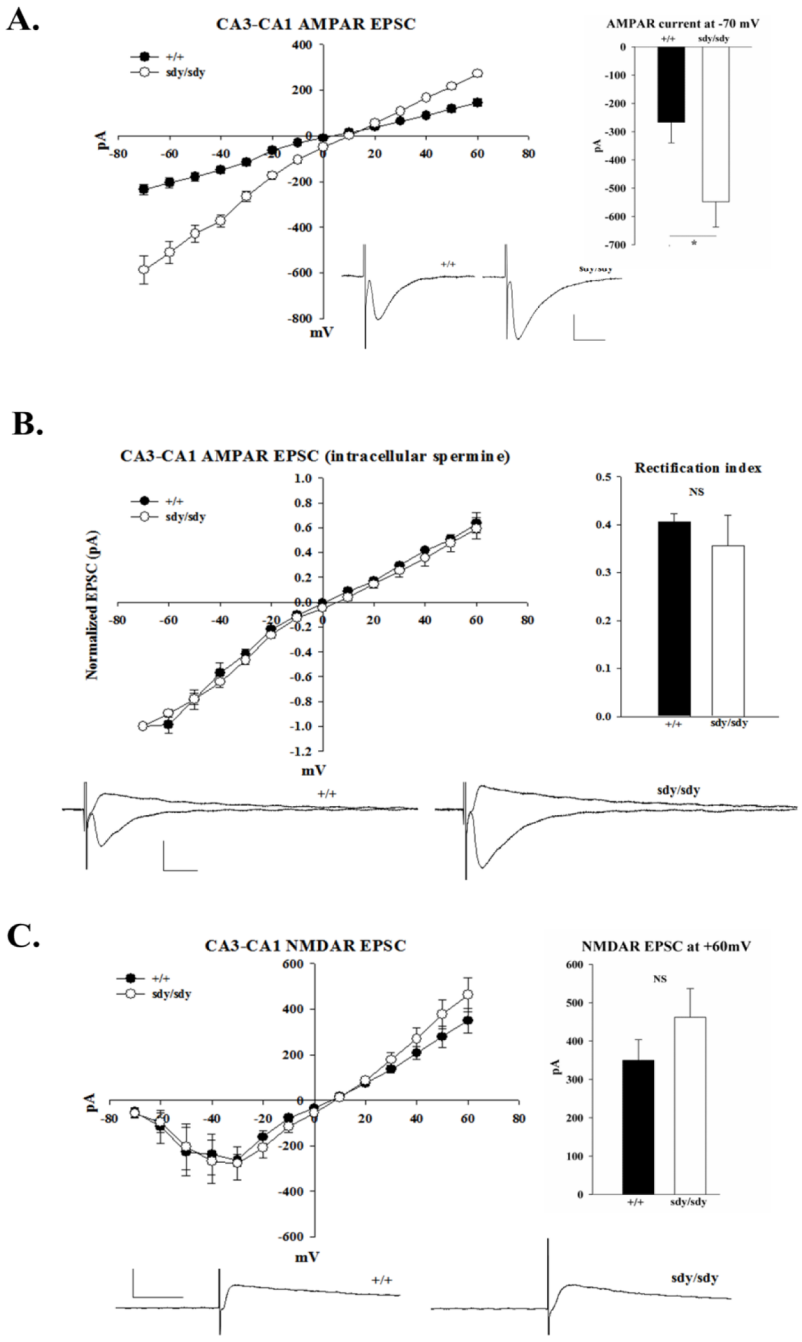

Figure 3. Enhanced CA3-CA1 AMPAR mediated transmission in sdy/sdy mice

A. Peak currents of evoked whole cell CA3-CA1 AMPAR EPSCs from P14–17 +/+ (n = 7 cells) and sdy/sdy mice (n = 7 cells) was plotted as a function of voltage. 10 μM bicuculline and 50 μM D-APV were present in the bath solution during recordings. The bar graph displays the values of the average peak current obtained at V_h: −70mV. B. Current voltage relations of AMPAR EPSCs were obtained from +/+ (n = 3 cells) and sdy/sdy (n = 4 cells) with 100 μM spermine in the patch pipette. EPSC amplitudes were normalized to the value obtained at V_h: −70mV for each respective genotype. The rectification index was calculated as the ratio of peak EPSC currents obtained at V_h: +40mV and V_h: −70mV. C. The peak current of whole cell CA3-CA1 NMDAR EPSCs from +/+ (n = 5 cells) and sdy/sdy (n = 5

cells) mice was plotted as a function of voltage. Recordings were done with 10 μM bicuculline and 10μM CNQX present in the bath solution. The bar graph displays the values of the average peak current obtained at V_h +60mV. Reported values represent mean ± SEM. Statistical analysis was performed using the Mann-Whitney test. An asterisk denotes $p<0.05$ while NS denotes data were not significant.

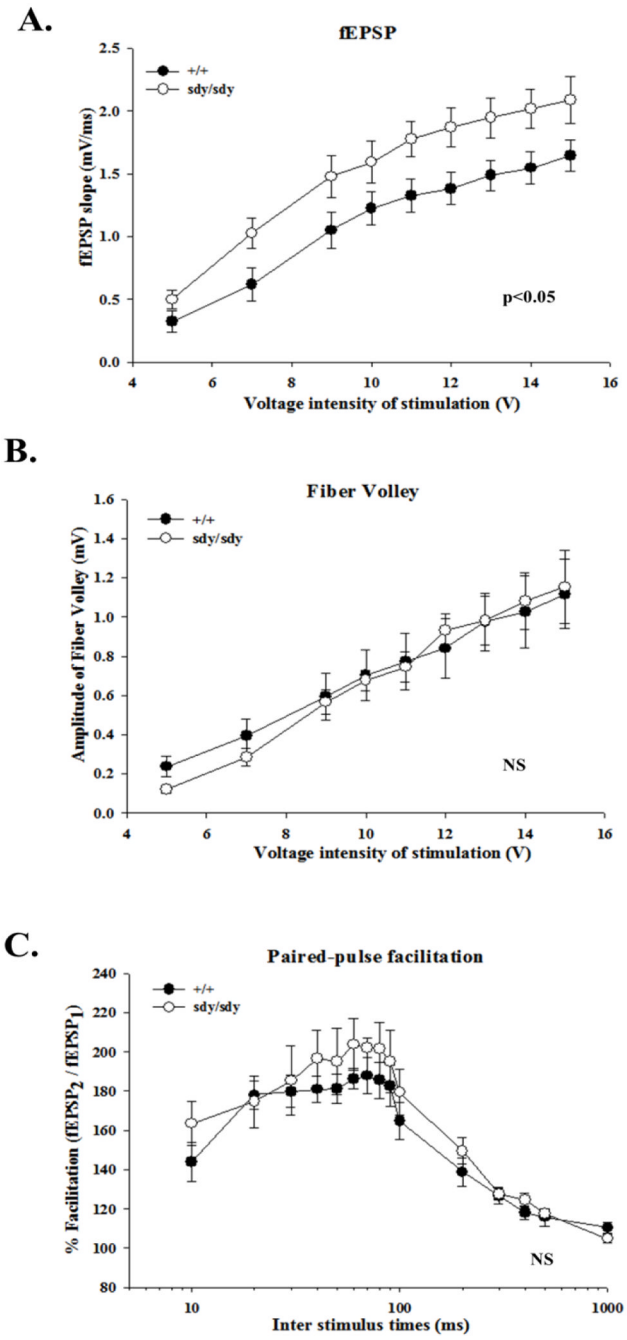

Figure 4. Enhanced CA3-CA1 basal synaptic transmission in sdy/sdy mice

A,B. The fEPSPs slopes and FV amplitudes obtained from P14–17 +/+ (n = 16 slices) and sdy/sdy mice (n = 10 slices) were plotted as a function of the voltage intensity of the stimulation. C. Percent facilitation ($100*fEPSP_2/fEPSP_1$) for +/+ (n = 11 slices) and sdy/sdy (n = 7 slices) mice was plotted as a function of the inter-stimulus times. Reported values represent mean ± SEM. Statistical analysis was performed using Two-Way ANOVA by genotype. NS denotes data were not significant.

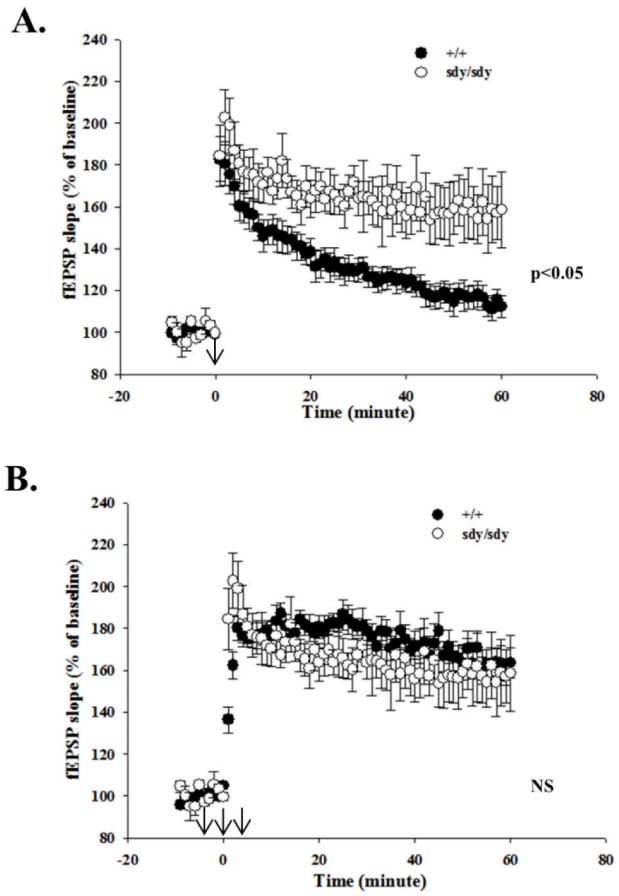

Figure 5. Enhanced CA3-CA1 LTP in sdy/sdy mice

A. The fEPSP slopes (% of baseline) following a 1x TBS stimulation of slices from P14–17 +/+ (n = 7) and sdy/sdy mice (n = 6 slices) were plotted as a function of time. See text for description of TBS. B. Plot of the fEPSP slopes (% of baseline) following a 3x TBS stimulation of slices for +/+ (n = 9) and sdy/sdy mice (n = 6 slices). Time = 0 signifies when the slices were tetanized. Reported values represent mean ± SEM. Statistical analysis was performed using the Mann-Whitney test and Two-Way ANOVA by genotype. NS denotes data were not significant.